ACS APPLIED MATERIALS & INTERFACES

Research Article

www.acsami.org

Silica Nanoparticle Doped Organic Ionic Plastic Crystal Electrolytes for Highly Efficient Solid-State Dye-Sensitized Solar Cells

Chengzhen Shi, Lihua Qiu, Xiaojian Chen, Haigang Zhang, Lei Wang, and Feng Yan*

Jiangsu Key Laboratory of Advanced Functional Polymer Design and Application, Department of Polymer Science and Engineering, College of Chemistry, Chemical Engineering and Materials Science, Soochow University, Suzhou, 215123, PR China

ABSTRACT: Organic ionic plastic crystal, 1-propyl-1-methylpyrrolidinium iodide ($P_{13}I$), which possesses a broad plastic phase from −36 to 135 °C, was doped with silica nanoparticles (SiO_2 NPs) and 1-ethyl-3-methylimidazolium iodide (EMII), for the preparation of SiO_2/EMII/$P_{13}I$ solid-state electrolytes for dye-sensitized solar cells (DSSCs). The thermal properties of all the electrolytes, including solid−solid phase transitions and melting temperatures, were investigated by differential scanning calorimetry (DSC). The effect of silica particles on the ionic conductivity, diffusion of I^-/I_3^- redox couple in electrolytes, and photovoltaic performance for solid-state DSSCs were investigated. The fabricated solid-state DSSCs yielded a high power conversion efficiency of 5.25% under simulated air mass 1.5 solar spectrum illuminations at 50 mW cm^{-2}. Furthermore, the DSSCs based on SiO_2/EMII/$P_{13}I$ solid-state electrolytes show good stability after an accelerating aging test, demonstrating potential practical applications.

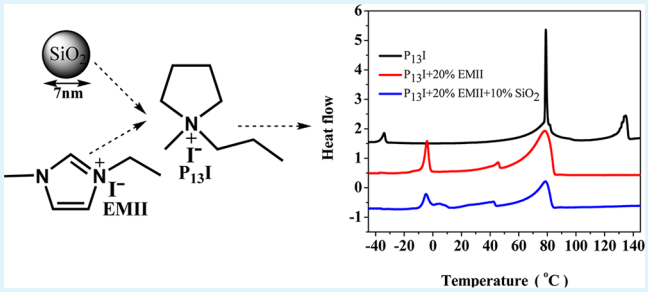

KEYWORDS: *plastic ionic crystals, SiO_2 nanoparticles, dye-sensitized solar cells, solid-state electrolyte, stability*

INTRODUCTION

Dye-sensitized solar cells (DSSCs) have been considered as feasible alternatives to silicon-based photovoltaic cells because of their ease of fabrication, low cost, and high power conversion efficiency.[1] Although the overall photoelectric conversion efficiency of the liquid electrolyte-based DSSCs has already achieved up to 12.3%,[2] the leakage and evaporation of organic solvent hinder the practical application of the DSSCs.[3] Various approaches, such as use of organic hole conductors,[4] physically cross-linked gelators,[5] and polymer gel electrolytes,[1c,6] have been devoted to developing (quasi-) solid-state electrolytes for the fabrication of DSSCs. However, poor solid-state electrolyte/electrode interfacial contact often resulted in low photoelectric conversion efficiency.[7] Therefore, development of solid-state electrolytes with high ionic conductivity and good pore filling property is critical for highly efficient solid-state DSSCs.

Organic plastic crystals are a type of material composed of organic molecules with long-range order and short-range rotational disorder.[8] A typical feature of organic plastic crystals is one or more solid−solid phase transitions below the melting point.[9] These solid−solid phase transitions enable plastic crystals with both plastic properties and good mechanical flexibility. Therefore, they can be deformed easily without fracture under a suitable applied force.[10] Although the conduction mechanism of the organic plastic crystals is still not fully understood, it is believed that the ionic conduction may be determined (at least in part) by lattice defects and rotation of molecules associated with the plastic phases.[8a,10,11] Therefore, organic plastic crystals have been considered as potential (quasi-) solid-state electrolytes for electrochemical devices, such as lithium batteries, fuel cells, and DSSCs,[12] because they can facilitate both high ionic conductivity and good electrode/electrolyte interfacial contact in the plastic phases. For example, a molecular plastic crystal, succinonitrile, based solid-state DSSC could achieve power conversion efficiencies exceeding ∼5% at full sunlight.[12b] However, a relatively low melting point of succinonitrile (∼57 °C) limited their application. Therefore, synthesis of organic ionic plastic crystals with high melting point (>60 °C) is highly desirable for the preparation of solid-state DSSCs.[13]

It has been demonstrated that a relatively high conductivity and rapid diffusion of redox couple through the electrolytes are critical to the solar cell performance.[12c] Therefore, the enhancement in conductivity of plastic crystal electrolytes upon addition of inorganic fillers has been studied because of the increased number of mobile defects induced in the electrolytes.[8a,13,14] In this paper, we report the application of organic ionic plastic crystals, instead of molecular plastic crystal (such as succinonitrile), as the electrolytes for solid-state DSSCs. 1-Propyl-1-methylpyrrolidinium iodide ($P_{13}I$), an organic ionic plastic crystal, was synthesized and first applied as the solid-state electrolyte for DSSCs. To increase the conductivity of the electrolytes, $P_{13}I$ was doped with silica nanoparticles (SiO_2 NPs). The effect of SiO_2 NPs on the ionic conductivity, diffusion of I^-/I_3^- redox couple in the electrolytes, and photovoltaic data for DSSCs was investigated. The

Received: December 1, 2012
Accepted: February 5, 2013
Published: February 5, 2013

fabricated solid-state DSSCs yielded the power conversion efficiency of 5.25% under simulated air mass 1.5 solar spectrum illuminations at 50 mW cm^{-2}. In addition, the resultant devices displayed good stability, indicating that the SiO_2/EMII/$P_{13}I$ solid electrolyte is a promising candidate for solar cells with good durability.

EXPERIMENTAL SECTION

Materials. 1-Iodopropane, 1-iodoethane, 1-methylpyrrolidine, and 1-methylimidazole were purchased from Alfa Aesar. The silica nanoparticles (~7 nm in diamater) were purchased from Degussa. $TiCl_4$ and H_2PtCl_6 were purchased from Aldrich. *cis*-Bis-(isothiocyanato) bis(2,20-bipyridyl-4,40-dicarboxylato) ruthenium(II) ([RuL_2 $(NCS)_2$]) was purchased from Solaronix SA (Switzerland) and used without any further purification. 1-Ethyl-3-methylimidazolium iodide (EMII) was synthesized according to the previous report.[15]

Synthesis of Organic Ionic Plastic Crystals. 1-Propyl-1-methylpyrrolidinium iodine ($P_{13}I$) was synthesized as follows: 4.0 g (47.0 mmol) of 1-methylpyrrolidine was dissolved in 25 mL of acetonitrile. Then 8.20 g (48.0 mmol) of 1-iodoethane was added dropwise into the prepared 1-methylpyrrolidine solution. The mixture was stirred at 40 °C for 24 h. Then the solvent was removed, and the solid product $P_{13}I$ was washed with ethyl acetate and dry diethyl ether three times. The produced $P_{13}I$ was dried under vacuum at room temperature to give a white solid: 11.52 g (96% yield). ^1H NMR: (400 MHz, D_2O) 3.45 (s, 4H), 3.24 (t, 2H), 2.99 (s, 3H), 2.16 (s, 4H), 1.76 (m, 2H), 0.94 (t, 3H).

Preparation of Electrolytes. The composition of all the solid-state electrolytes is listed in Table 1. The plastic ionic crystal-based electrolytes were prepared in a nitrogen glovebox. The mixture containing EMII, $P_{13}I$, SiO_2, and I_2 was stirred at 80 °C for 2 h and then allowed to cool to room temperature to give a solid-state electrolyte before the characterization and fabrication of DSSCs.

Table 1. Component of the Electrolytes Applied for the DSSCs

electrolyte	matrix	7 nm SiO_2	I_2
electrolyte-A	$P_{13}I$ + 10 wt % EMII	0 wt %	0.2 M
electrolyte-B	$P_{13}I$ + 20 wt % EMII	0 wt %	0.2 M
electrolyte-C	$P_{13}I$ + 20 wt % EMII	5 wt %	0.2 M
electrolyte-D	$P_{13}I$ + 20 wt % EMII	10 wt %	0.2 M

Characterization of the Electrolytes. ^1H NMR spectra were recorded on a Varian 400 MHz spectrometer. The thermal properties of electrolytes were measured on a Perkin-Elmer DSC 4000 at a scanning rate of 5 °C min^{-1} under N_2 atmosphere. The conductivity of electrolytes was characterized in a cell composed of a Teflon tube and two identical stainless steel electrodes on a CHI660c electrochemical workstation under a N_2 atmosphere. All the samples were equilibrated for at least 30 min at a given temperature. Steady-state voltammetry was tested in a photoelectrochemical cell equipped with a platinum ultramicroelectrode (~10 μm in diameter) and platinum foil as the working and counter electrode, respectively. The electrochemical impedance spectra (EIS) of all the devices were tested using a CHI 660c electrochemical workstation under the dark. The bias voltage for the impedance measurement was −0.70 V, and the frequency ranged from 0.01 to 10^5 Hz.

Device Fabrication and Characterization.[16] The cleaned FTO glass was covered at two parallel edges with an adhesive tape to control the thickness of mesoporous TiO_2 film. Two layers of TiO_2 particles were deposited onto cleaned FTO glass and used as photoelectrodes. A 10 μm thick film of 20 nm sized TiO_2 particles was deposited onto the FTO glass electrode by the doctor-blade technique. The film was dried at 125 °C for 5 min. Then, a second 5 μm thick layer of 200 nm light scattering anatase particles was coated on the top of the first TiO_2 layer. The resulting TiO_2 films were annealed at 500 °C for 30 min. After cooling to 80 °C, the obtained TiO_2 electrode was immersed in 0.5 mM Z-907 acetonitrile and *tert*-butyl alcohol solution at room temperature for 24 h to complete the sensitizer loading. The dye-sensitized TiO_2 electrode was washed with anhydrous ethanol and dried with a nitrogen stream. To prepare the Pt counter electrode, two drops of 5 mM H_2PtCl_6 in ethanol were placed onto the cleaned FTO glass substrate with a diameter of 1 mm hole, followed by drying and annealing at 400 °C for 15 min.

The DSSCs were fabricated by sandwiching solid-state electrolytes between a dye-sensitized TiO_2 electrode and a Pt counter electrode, which were separated by a 25 μm thick hot melt ring (Surlyn, Dupont) and sealed by heating. The methanol solution of solid-state electrolyte (30 wt %) was injected into the sandwiched cells using a vacuum backfilling system. The cells were then heated to 80 °C under vacuum to remove methanol and residual air from the electrolyte. This procedure was repeated several times to remove the residual methanol to guarantee optimal filling and fine electrical contact. The electrolyte injection hole on the thermally platinized FTO counter electrode was finally sealed with a Surlyn sheet and a thin glass by heating. The fabricated DSSCs shielded by an aluminum foil mask with an aperture area of ~0.1 cm^2 were stored in a chamber at 30 °C, and the photocurrent density−voltage (J−V) curves were measured with a digital source meter (Keithley, model 2400) under simulated air mass (AM) 1.5 solar spectrum illumination at 15, 50, and 100 mW cm^{-2}, respectively. Incident photon-to-current conversion efficiency (IPCE) plotted as a function of excitation wavelength was recorded on a Keithley 2400 source meter under the irradiation of a Xenon lamp with a monochromator (Oriel Cornerstone TM 260 1/4).

RESULTS AND DISCUSSION

Thermal and Electrical Properties of Electrolytes. Figure 1a shows the typical thermal analysis traces for pure

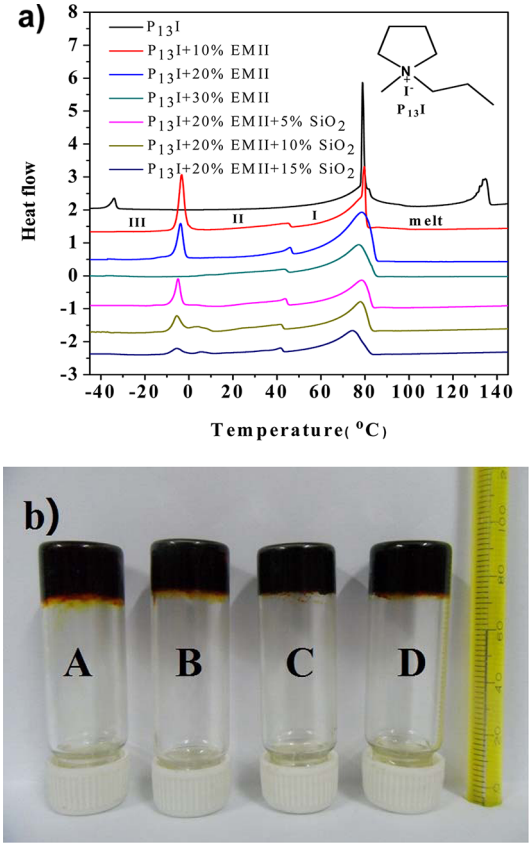

Figure 1. (a) Differential scanning calorimetric (DSC) thermograms for EMII and SiO_2 NP doped $P_{13}I$ electrolytes. (b) Photograph of the solid-state electrolytes A−D at 60 °C.

dx.doi.org/10.1021/am302925s | ACS Appl. Mater. Interfaces 2013, 5, 1453−1459

Table 2. Onset Temperature and Entropy Change for Phase Transitions of Different Electrolyte Samples

	III to II		II to I		I to melt	
	T	ΔS	T	ΔS	T	ΔS
electrolytes	(°C)	(J kmol^{-1})	(°C)	(J kmol^{-1})	(°C)	(J kmol^{-1})
$P_{13}I$ + 10% EMII	−4.3	30.8	42.3	4.4	71.6	39.2
$P_{13}I$ + 20% EMII	−5.2	19.6	42.5	4.3	71.4	35.5
$P_{13}I$ + 30% EMII			42.4	3.8	69.5	34.2
$P_{13}I$ + 20% EMII + 5% SiO_2	−5.9	15.2	42.5	4.2	71.0	33.2
$P_{13}I$ + 20% EMII + 10% SiO_2	−6.7	12.8	41.3	4.1	66.9	24.5
$P_{13}I$ + 20% EMII + 15% SiO_2	−7.2	7.5	41.0	3.6	64.2	16.8

and the EMII (or SiO_2 NPs) doped $P_{13}I$ electrolytes. The pure $P_{13}I$ shows two solid−solid phase transformations at −36 °C (entropy of transition 5.1 J K mol^{-1}) and 78 °C (entropy of transition 38.5 J K mol^{-1}) and a melting point at 135 °C (entropy of transition 8.1 J K mol^{-1}), respectively. In this work, EMII was chosen to dope $P_{13}I$ for the formation of plastic crystal electrolytes with high conductivity. It can be clearly seen that the phase transition temperatures of solid−solid transitions and melting point were drastically changed upon the addition of EMII. Compared with pure $P_{13}I$, the solid−solid transition temperatures of 20 wt % EMII-doped $P_{13}I$ electrolytes was changed from −36 and 78 °C to −5 and 42.5 °C, respectively, and the melting temperature was decreased from 135 to 78 °C. It should be noted that the III → II transition decreases in intensity with the further addition of SiO_2 NPs, and the melt transition is skewed for the composite electrolytes (Figure 1a). However, the solid−solid transition of $P_{13}I$ almost disappeared after being doped with 30 wt % EMII probably due to the disruption of the $P_{13}I$ plastic crystal bulk matrix. It is interesting that further addition of SiO_2 NPs did not affect the thermal properties of the electrolytes. Similarly, the solid−solid transition of the electrolytes containing 20 wt % EMII and 15 wt % SiO_2 NPs almost disappeared, indicating a disruption of the $P_{13}I$ plastic crystal bulk matrix.

The onset transition temperature as well as the entropy changes of composite samples are summarized and listed in Table 2. It can be seen that the onset temperatures of solid−solid transitions were basically shifted toward lower temperatures, and the entropy changes of the phase transitions decreased with the increasing content of EMII and SiO_2 NPs. These results indicate that EMII and SiO_2 NPs have been incorporated into the bulk matrix of $P_{13}I$ to form a solid solution. The typical decrease in the ΔS of phase transitions might be due to the appearance of defected/amorphous regions in the plastic crystals.[8a] It should be noted that all the plastic crystal electrolyte samples were solid state below 60 °C (Figure 1b).

Figure 2 shows the ionic conductivity of the electrolytes in the measured temperature region (25−80 °C), and the results are summarized in Table 3. It can be clearly seen that the conductivity of all the electrolytes increased with increasing temperature and EMII content. For example, the conductivity of electrolyte-B (doped with 20 wt % EMII) is higher than that of electrolyte-A (doped with 10 wt % EMII). Further addition of SiO_2 NPs could drastically increase the conductivity of the electrolytes. The conductivity of electrolyte-C and electrolyte-D was improved to 2.71 × 10^{-4} and 5.65 × 10^{-4} S cm^{-1}, respectively, if compared with that of electrolyte-A (1.23 × 10^{-4} S cm^{-1}) and electrolyte-B (2.09 × 10^{-4} S cm^{-1}). The increase in conductivity is closely related to the increase in the size and number of defects formed in the matrix.[14,17] Therefore, it is

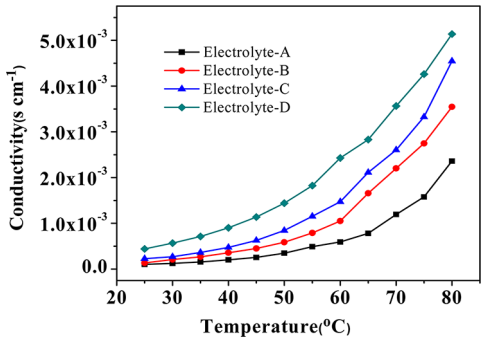

Figure 2. Conductivity−temperature plots for the four electrolytes.

assumed that addition of EMII and SiO_2 NPs into the plastic crystal bulk matrix increases the number and size of mobile defects, which enhance the conductivity of electrolytes.

Figure 3 shows the comparative steady-state voltammograms of four plastic crystal electrolytes at 30 °C. The apparent diffusion coefficients (D_{app}) of the I^-/I_3^- redox couple were calculated from the anodic and cathodic steady-state currents (I_{ss}) using the following equation[18]

$$I_{ss} = 4nFD_{app}C\gamma$$

where n is the number of electrons per molecule; F is the Faraday constant; γ is the radius of the ultramicroelectrode; and C is the bulk concentration of the electroactive species. The calculated values of D_{app} are also summarized in Table 3.

The D_{app} values of iodide and triiodide of electrolyte-B at 30 °C were determined to be 6.84 × 10^{-7} and 1.33 × 10^{-6} cm^2 s^{-1} (Table 3), respectively. It can be clearly seen that the D_{app} of iodide and triiodide increases with the increment of EMII content from the electrolyte-A to electrolyte-B. The high ion diffusivity of the doped $P_{13}I$ plastic crystal electrolytes might be due to the decoupling of rotational disorder and the existence of vacancies in the lattice, which probably originated from the local defect rotations in the $P_{13}I$ plastic crystal above the solid−solid transformation temperature.[19]

However, it should be noted that electrolyte-C and electrolyte-D show lower diffusion coefficients of triiodide (I_3^-) than that of electrolyte-B, while the value of iodide (I^-) diffusion coefficients is almost unchanged (Table 3). Similar results have been observed by Chen et al. although the mechanism is still not fully understood.[20] Our understanding is that the lowered diffusion coefficients of triiodide might be due to the disordered distribution caused by the aggregation of SiO_2 NPs in the electrolytes, which hindered the diffusion of iodide and triiodide in the channels formed through the SiO_2 NP network. Since the volume of iodide is quite smaller than that of triiodide, the diffusion inhibition of iodide is relatively

Table 3. Ionic Conductivity and Apparent Diffusion Coefficients (D_{app}) of Iodide and Triiodide in the Different Electrolytes at 30 °C

electrolyte	conductivity/S cm^{-1}	D_{app} (I_3^-)/cm^2 s^{-1}	D_{app} (I^-)/cm^2 s^{-1}
electrolyte-A	1.23×10^{-4}	1.10×10^{-6}	2.68×10^{-7}
electrolyte-B	2.09×10^{-4}	1.33×10^{-6}	6.84×10^{-7}
electrolyte-C	2.71×10^{-4}	7.36×10^{-7}	6.73×10^{-7}
electrolyte-D	5.65×10^{-4}	6.44×10^{-7}	8.65×10^{-7}

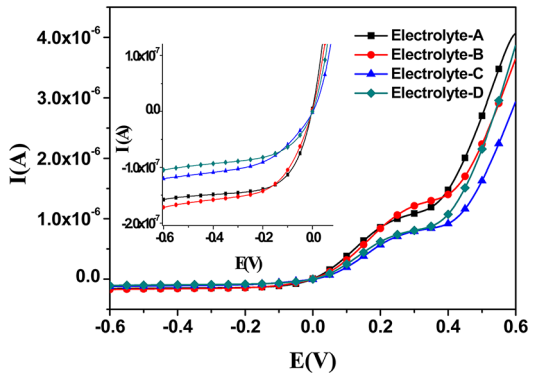

Figure 3. Steady-state voltammograms of a platinum ultramicroelectrode (~10 μm in diameter) in four electrolytes at 30 °C. Scan rate: 10 mV s^{-1}.

weaker and even can be omitted. As a result, the D_{app} (I^-) of electrolyte-C and electrolyte-D is approximately unchanged, while the value of D_{app} (I_3^-) is drastically decreased.

It is noteworthy that the conductivity changes of four electrolytes are inconsistent with the variation tendency of diffusion rates of I_3^- and I^- ions because the rotation, hop, and diffusion of cations (such as 1-propyl-1-methylpyrrolidinium cations) involved in the plastic phases also contribute to the overall ionic conductivity of the electrolytes.[11b] Similar results have been observed by Zhou and co-workers.[5]

The charge transport in such a solid-state electrolyte could be interpreted as the Grotthus-type electron-exchange mechanism and be expressed by the Dahms–Ruff equation.[21]

$$D_{app} = D_{phys} + k_{ex}\delta^2 c/6$$

where D_{phys} is physical diffusion; k_{ex} is the rate constant of electron exchange; and c and δ are the concentration and average center-to-center distances between redox species, respectively. It has been recently demonstrated via electrochemical analysis that the charge transport is solely based on the physical diffusion at the ratio of $[I^-]/[I_2] = 10$.[21b] Here, the same ratio of $[I^-]/[I_2]$ was applied in the electrolytes, and thus the charge transportation is conducted predominantly via physical diffusion (D_{phys}). Addition of SiO_2 NPs in the electrolytes blocked some of the possible diffusion paths that cause the decrease of D_{phys} values, and thus it is not surprising that the D_{app} value of triiodide in electrolyte-D was decreased from 1.33×10^{-6} to 6.44×10^{-7} cm^2 s^{-1}.

Characterization of DSSCs. Photocurrent density–voltage (J–V) characteristics of the devices measured under standard AM 1.5 solar illumination at an intensity of 100 mW cm^{-2} are shown in Figure 4. The data of the open-circuit voltage (V_{oc}), short-circuit current density (J_{sc}), fill factor (FF), and the overall photoelectric conversion efficiency (PCE) of the DSSCs are also summarized and listed in Table 4. The influence of the dopants on the photovoltaic parameters of DSSCs was first investigated at 30 °C. It can be clearly seen that the value of J_{sc}

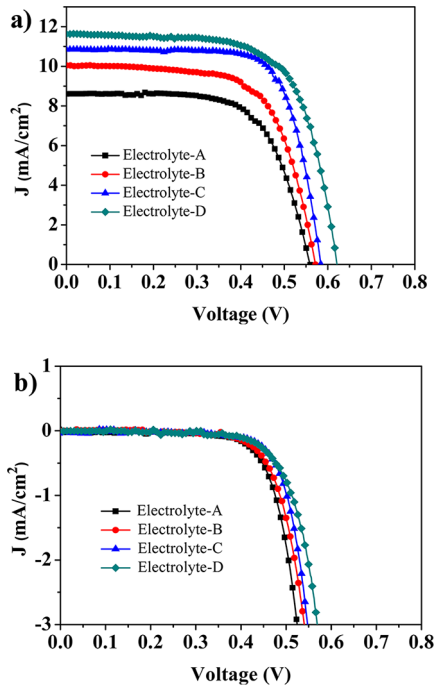

Figure 4. J–V curves of DSSCs containing electrolyte-A, B, C, and D at 30 °C (a) under simulated AM 1.5 solar spectrum irradiation at 100 mW cm^{-2} (cells are tested using an aluminum foil mask with an aperture area of 0.1 cm^2) and (b) in the dark.

Table 4. Performance Parameters of DSSCs with Different Electrolytes at 30 °C

electrolyte	V_{oc}/V	J_{sc}/mA cm^{-2}	FF	PCE (%)
electrolyte-A	0.560	8.61	0.663	3.19
electrolyte-B	0.572	10.05	0.660	3.79
electrolyte-C	0.584	10.85	0.703	4.45
electrolyte-D	0.622	11.62	0.677	4.90

significantly increased with the increase of EMII and SiO_2 NP content due to the enhanced ionic conductivity. In addition, the V_{oc} of electrolyte-C and electrolyte-D was increased from 0.572 to 0.584 and 0.622 V, respectively, probably due to the suppressed dark current upon the addition of SiO_2 NPs (Figure 4b). Therefore, the cell with electrolyte-D exhibited a V_{oc} of 0.622 V, a J_{sc} of 11.62 mA cm^{-2}, and a FF of 0.677, yielding a highest conversion efficiency of 4.90% at 30 °C.

It has been demonstrated that the dark current originates from the reduction of I_3^- by conduction band electrons from TiO_2.[16a] The decrease of the I_3^- reduction rate should lead to an increase of V_{oc} according to the following equation[16a,b]

$$V_{oc} = \frac{kT}{e} \ln\left(\frac{I_{inj}}{n_{cb} k_{et} [I_3^-]}\right)$$

where I_{inj} is the flux of charge resulting from sensitized injection related to the electron back transfer rate; n_{cb} is the concentration of electrons at the TiO_2 surface; and k_{et} is the rate constant for I_3^- reduction.

As shown in Figure 4b, the onset of the dark current is negatively shifted by approx 30 mV from electrolyte-D to electrolyte-B (at the current density of −3 mA/cm^2) due to the lower I_3^- reduction rate (k_{et}). Addition of SiO_2 NPs reduces the D_{app} of I_3^-, leading to an increase of the possibility that I_3^- ions capture the electron. As it has already been demonstrated that the 10 μm thick 20 nm sized TiO_2 films could form the pores with the average diameter of ∼22 nm after being dried and annealed at 500 °C,[22] therefore, ∼7 nm SiO_2 NPs applied in this work may enter in the pores as well as be distributed on the surface of the TiO_2 film to inhibit the back reaction.[16f] The reduction rate of I_3^- (k_{et}) will thus be decreased and lead to an enhancement of V_{oc} values. Therefore, the electrolyte-D based cell shows a higher V_{oc} (0.622 V) and a higher PCE (4.90%) as compared with electrolyte-B.

Electrochemical impedance spectra (EIS) were then applied to investigate the interfacial charge transfer processes of the devices at 30 °C (Figure 5). Figure 5a shows the Nyquist plots

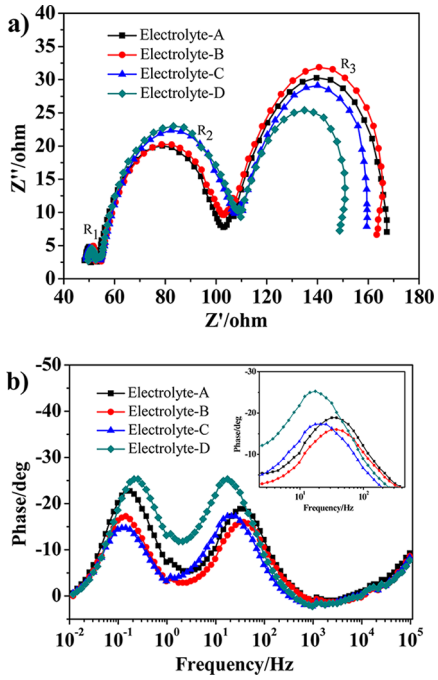

Figure 5. (a) Nyquist plots of the electrochemical impedance spectra measured for DSSCs based on electrolytes A–D. (b) Fitted Bode phase plots of each device. The bias voltage for the impedance measurement was −0.70 V, and the frequency ranged from 0.01 to 10^5 Hz in the dark.

of the electrochemical impedance spectra measured for DSSCs based on electrolytes A–D. From high to low frequency, three characteristic arcs of R_1, R_2, and R_3 represent the resistance of the Pt counter electrode/electrolyte interface, TiO_2/electrolyte interface, and the Nernst diffusion in the electrolyte, respectively.[12c] It can be clearly seen that the Nyquist plots show distinctly nonsemicircular behavior. This somewhat distorted behavior is generally attributed to "stretched exponential" behavior, meaning there are a distribution of relaxation times. The bigger the distorted semicircle in the intermediate-frequency region, the weaker the electron recombination at the TiO_2/electrolyte interface.[23] Here, it can be seen that the TiO_2/electrolyte (R_2) resistance increased with the addition of SiO_2 NPs. This result is consistent with that of the dark current characterization. In addition, the value of R_3 decreases with the addition of SiO_2 NPs, indicating an increase of the conductivity of the electrolyte.

Figure 5b shows the Bode phase plots of the EIS spectra which displayed the characteristic frequency peaks of the charge transfer process for all the cells. The low-frequency and middle-frequency peaks observed in the Bode phase plots correspond to a diffusion process in the electrolyte and carrier recombination process photoanode/electrolyte interface, respectively. The effective lifetime of electrons (τ_e) before recombination in the TiO_2 photoelectrode can be related to the inverse of the characteristic frequency and is estimated by the following equation[24]

$$\tau_e = \frac{1}{\omega_{mid}} = \frac{1}{2\pi f_{mid}}$$

where ω_{mid} is the frequency angle of the middle-frequency peak and f_{mid} is the frequency of the middle-frequency peak. The f_{mid} and lifetime of electrons are also summarized in Table 5.

Table 5. Parameters Obtained by Fitting the EIS of the DSSCs Fabricated with Four Electrolytes

electrolyte	R_1/Ω	R_2/Ω	R_3/Ω	f_{mid}/Hz	τ_e/ms
electrolyte-A	4.17	46.14	58.07	26.24	6.07
electrolyte-B	3.92	48.10	56.37	25.51	6.24
electrolyte-C	4.02	53.06	50.12	19.17	8.30
electrolyte-D	3.74	55.72	44.15	14.52	10.98

The electron lifetime for recombination (τ_e) of the cell with electrolyte-A gives the lowest value of 6.07 ms, while the cell with electrolyte-D shows the highest value of 10.98 ms. Compared with electrolyte-B, the cell with electrolyte-D shows a higher recombination resistance and a longer electron lifetime, which favors electron transport through a longer distance with less diffusive hindrance and finally leads to enhanced photoconversion efficiency.[24] Therefore, it can be concluded that the SiO_2 NPs in solid electrolytes decreased electron recombination, leading to enhanced electron transfer, and further increased cell performance. In addition, the low-frequency peak of the cell with electrolyte-D shifted to higher frequency (Figure 5b) if compared with electrolyte-B, indicating an increase in the ion diffusion of the electrolyte. The result is consistent with the decrease of the diffusion resistance in the electrolyte-D (R_3).

The incident photon-to-current conversion efficiency (IPCE) values of devices based on four electrolytes are shown in Figure 6. The maximum IPCE values at 530 nm are 51%, 60%, 66%, and 68% for the cells with electrolyte-A, B, C, and D, respectively. The IPCE values increased with the addition of SiO_2 NPs, which is consistent with the variation tendency of J_{sc}. A broad feature appears to cover the visible spectrum range from 450 to 650 nm. The PCE of the devices under different light intensity illumination are also summarized in Table 6. The PCE at 1.0 sunlight is lower than that at 0.5 sunlight, probably due to the inefficient charge screening of electron transport within the TiO_2 film,[12b] while the PCE at 0.15 sunlight is lower than that at 0.5 sunlight because of the photocurrent response

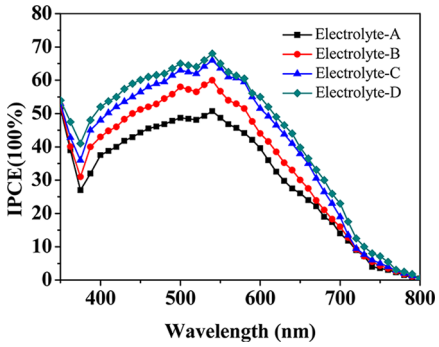

Figure 6. IPCE vs wavelength profiles for cells based on electrolytes A–D.

Table 6. PCE of DSSCs Based on Different Electrolytes under Simulated AM 1.5 Solar Irradiation

	PCE under different incident light intensity irradiations (%)		
electrolyte	1.0 sun	0.5 sun	0.15 sun
electrolyte-A	3.19	3.74	3.52
electrolyte-B	3.79	4.10	3.94
electrolyte-C	4.45	4.98	4.73
electrolyte-D	4.90	5.25	5.08

to light intensities and the changes in performance parameters.[6b] The DSSC based on electrolyte-D shows a maximum PCE value of 5.25% under AM 1.5 irradiance at 50 mW cm^{-2}.

The long-term stability of the fabricated DSSCs with four electrolytes was investigated via an accelerating aging test of sealed devices. The cells were stored in a chamber at 30 °C, covered with an UV cutoff filter, and irradiated at open circuit under one sun visible-light soaking. The PCE of the cells is measured every four days, and the total efficiencies are normalized to the values measured on the first day (Figure 7). During the first eight days, the efficiency was moderately

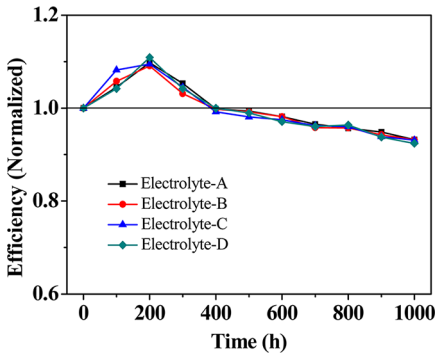

Figure 7. PCEs of DSSCs containing solid-state electrolytes as a function of time at 30 °C with successive one sun visible-light soaking.

enhanced probably due to an increase of the regeneration of dye Z907 and thus an increase of J_{sc}.[25] All the solid-state electrolyte cells maintained about 92% of the initial PCE values after 1000 h test. These results mean that addition of SiO_2 NPs to the electrolytes did not affect the long-term stability of solar cell devices. These results further confirmed the good stability of plastic ionic crystal based solid-state DSSCs fabricated in this work.

CONCLUSIONS

In summary, SiO_2 NP doped organic ionic plastic crystal electrolytes have been prepared and employed for solid-state DSSCs. The SiO_2/EMII/P_{13}I solid-state electrolytes are solid below 60 °C and the conductivity increase upon the addition of SiO_2 NPs. The fabricated solid-state electrolyte DSSCs showed an efficiency of 5.25% under simulated air mass 1.5 solar spectrum illumination at 50 mW cm^{-2} and good stability. The results of this study suggest that solid-state DSSCs based on SiO_2 NP doped organic ionic plastic crystal solid-state electrolytes could overcome the leakage problem of devices with liquid electrolytes.

AUTHOR INFORMATION

Corresponding Author

*E-mail: fyan@suda.edu.cn.

Notes

The authors declare no competing financial interest.

ACKNOWLEDGMENTS

This work was supported by Natural Science Foundation of China (Nos. 21174102, 21274101), The Natural Science Foundation of Jiangsu Province (BK2011274), Program for Scientific Innovation Research of College Graduate in Jiangsu Province (CXZZ11-0103), and the Project Funded by the Priority Academic Program Development of Jiangsu Higher Education Institutions.

REFERENCES

(1) (a) O'Regan, B.; Gratzel, M. *Nature* **1991**, *353*, 737–740. (b) Armel, V.; Forsyth, M.; MacFarlane, D. R.; Pringle, J. M. *Energy Environ. Sci.* **2011**, *4*, 2234–2239. (c) Chen, X.; Li, Q.; Zhao, J.; Qiu, L.; Zhang, Y.; Sun, B.; Yan, F. *J. Power Sources* **2012**, *207*, 216–221. (d) Wang, H.; Zhang, X.; Gong, F.; Zhou, G.; Wang, Z.-S. *Adv. Mater.* **2012**, *24*, 121–124. (e) Chen, W.-C.; Chen, C.-Y.; Wu, C.-G.; Ho, K.-C.; Wang, L. *J. Power Sources* **2012**, *214*, 113–118. (f) Liu, R.; Yang, W.-D.; Qiang, L.-S.; Liu, H.-Y. *J. Power Sources* **2012**, *220*, 153–159. (g) Yang, H.; Yu, C.; Song, Q.; Xia, Y.; Li, F.; Chen, Z.; Li, X.; Yi, T.; Huang, C. *Chem. Mater.* **2006**, *18*, 5173–5177. (h) Zhao, Y.; Zhai, J.; He, J.; Chen, X.; Chen, L.; Zhang, L.; Tian, Y.; Jiang, L.; Zhu, D. *Chem. Mater.* **2008**, *20*, 6022–6028. (i) Jeon, S.; Jo, Y.; Kim, K.-J.; Jun, Y.; Han, C.-H. *ACS Appl. Mater. Interfaces* **2011**, *3*, 512–516.

(2) Yella, A.; Lee, H.-W.; Tsao, H. N.; Yi, C.; Chandiran, A. K.; Nazeeruddin, M. K.; Diau, E. W.-G.; Yeh, C.-Y.; Zakeeruddin, S. M.; Grätzel, M. *Science* **2011**, *334*, 629–634.

(3) Snaith, H. J.; Schmidt-Mende, L. *Adv. Mater.* **2007**, *19*, 3187–3200.

(4) Docampo, P.; Guldin, S.; Stefik, M.; Tiwana, P.; Orilall, M. C.; Hüttner, S.; Sai, H.; Wiesner, U.; Steiner, U.; Snaith, H. J. *Adv. Funct. Mater.* **2010**, *20*, 1787–1796.

(5) Zhou, Y.; Xiang, W.; Chen, S.; Fang, S.; Zhou, X.; Zhang, J.; Lin, Y. *Chem. Commun.* **2009**, 3895–3897.

(6) (a) Zhao, J.; Chen, X.; Yan, F.; Qiu, L.; Lee, S.; Sun, B. *J. Mater. Chem.* **2011**, *21*, 7326–7330. (b) Wang, M.; Pan, X.; Fang, X.; Guo, L.; Zhang, C.; Huang, Y.; Huo, Z.; Dai, S. *J. Power Sources* **2011**, *196*, 5784–5791.

(7) Bach, U.; Lupo, D.; Comte, P.; Moser, J. E.; Weissortel, F.; Salbeck, J.; Spreitzer, H.; Gratzel, M. *Nature* **1998**, *395*, 583–585.

(8) (a) Adebahr, J.; Seeber, A. J.; MacFarlane, D. R.; Forsyth, M. *J. Phys. Chem. B* **2005**, *109*, 20087–20092. (b) Golding, J.; Hamid, N.; MacFarlane, D. R.; Forsyth, M.; Forsyth, C.; Collins, C.; Huang, J. *Chem. Mater.* **2001**, *13*, 558–564.

(9) Henderson, W. A.; Young, V. G.; Passerini, S.; Trulove, P. C.; De Long, H. C. *Chem. Mater.* **2006**, *18*, 934–938.

(10) (a) Pringle, J. M.; Howlett, P. C.; MacFarlane, D. R.; Forsyth, M. *J. Mater. Chem.* **2010**, *20*, 2056−2062. (b) Pringle, J. M. *Phys. Chem. Chem. Phys.* **2013**, *15*, 1339−1351.
(11) (a) MacFarlane, D. R.; Forsyth, M. *Adv. Mater.* **2001**, *13*, 957−966. (b) Jin, L.; Nairn, K. M.; Forsyth, C. M.; Seeber, A. J.; MacFarlane, D. R.; Howlett, P. C.; Forsyth, M.; Pringle, J. M. *J. Am. Chem. Soc.* **2012**, *134*, 9688−9697.
(12) (a) Abu-Lebdeh, Y.; Alarco, P.-J.; Armand, M. *Angew. Chem., Int. Ed.* **2003**, *42*, 4499−4501. (b) Wang, P.; Dai, Q.; Zakeeruddin, S. M.; Forsyth, M.; MacFarlane, D. R.; Grätzel, M. *J. Am. Chem. Soc.* **2004**, *126*, 13590−13591. (c) Li, Q.; Zhao, J.; Sun, B.; Lin, B.; Qiu, L.; Zhang, Y.; Chen, X.; Lu, J.; Yan, F. *Adv. Mater.* **2012**, *24*, 945−950.
(13) Shekibi, Y.; Pringle, J. M.; Sun, J.; Pas, S. J.; Rocher, N. M.; Clare, B. R.; Hill, A. J.; MacFarlane, D. R.; Forsyth, M. *J. Mater. Chem.* **2010**, *20*, 338−344.
(14) Shekibi, Y.; Gray-Weale, A.; MacFarlane, D. R.; Hill, A. J.; Forsyth, M. *J. Phys. Chem. C* **2007**, *111*, 11463−11468.
(15) Bonhôte, P.; Dias, A.-P.; Papageorgiou, N.; Kalyanasundaram, K.; Grätzel, M. *Inorg. Chem.* **1996**, *35*, 1168−1178.
(16) (a) Nazeeruddin, M. K.; Kay, A.; Rodicio, I.; Humphry-Baker, R.; Mueller, E.; Liska, P.; Vlachopoulos, N.; Graetzel, M. *J. Am. Chem. Soc.* **1993**, *115*, 6382−6390. (b) Chen, X.; Zhao, J.; Zhang, J.; Qiu, L.; Xu, D.; Zhang, H.; Han, X.; Sun, B.; Fu, G.; Zhang, Y.; Yan, F. *J. Mater. Chem.* **2012**, *22*, 18018−18024. (c) Li, Q.; Chen, X.; Zhao, J.; Qiu, L.; Zhang, Y.; Sun, B.; Yan, F. *J. Mater. Chem.* **2012**, *22*, 6674−6679. (d) Jiang, X.; Karlsson, K. M.; Gabrielsson, E.; Johansson, E. M. J.; Quintana, M.; Karlsson, M.; Sun, L.; Boschloo, G.; Hagfeldt, A. *Adv. Funct. Mater.* **2011**, *21*, 2944−2952. (e) Ito, S.; Murakami, T. N.; Comte, P.; Liska, P.; Grätzel, C.; Nazeeruddin, M. K.; Grätzel, M. *Thin Solid Films* **2008**, *516*, 4613−4619. (f) Zhang, Z.; Zakeeruddin, S. M.; O'Regan, B. C.; Humphry-Baker, R.; Grätzel, M. *J. Phys. Chem. B* **2005**, *109*, 21818−21824.
(17) Hill, A. J.; Huang, J.; Efthimiadis, J.; Meakin, P.; Forsyth, M.; MacFarlane, D. R. *Solid State Ionics* **2002**, *154*, 119−124.
(18) (a) Dai, Q.; MacFarlane, D. R.; Howlett, P. C.; Forsyth, M. *Angew. Chem.* **2005**, *117*, 317−320. (b) Zhang, Y.; Zhao, J.; Sun, B.; Chen, X.; Li, Q.; Qiu, L.; Yan, F. *Electrochim. Acta* **2012**, *61*, 185−190.
(19) MacFarlane, D. R.; Huang, J.; Forsyth, M. *Nature* **1999**, *402*, 792−794.
(20) (a) Chen, Z.; Yang, H.; Li, X.; Li, F.; Yi, T.; Huang, C. *J. Mater. Chem.* **2007**, *17*, 1602−1607. (b) Lan, Z.; Wu, J.; Lin, J.; Huang, M. *Sci. China Chem.* **2010**, *53*, 1352−1357.
(21) (a) Kawano, R.; Watanabe, M. *Chem. Commun.* **2005**, 2107−2109. (b) Wang, X.; Kulkarni, S. A.; Ito, B. I.; Batabyal, S. K.; Nonomura, K.; Wong, C. C.; Grätzel, M.; Mhaisalkar, S. G.; Uchida, S. *ACS Appl. Mater. Interfaces* **2013**, *5*, 444−450.
(22) Wang, P.; Zakeeruddin, S. M.; Comte, P.; Exnar, I.; Grätzel, M. *J. Am. Chem. Soc.* **2003**, *125*, 1166−1167.
(23) Huo, Z.; Dai, S.; Wang, K.; Kong, F.; Zhang, C.; Pan, X.; Fang, X. *Sol. Energy Mater. Sol. Cells* **2007**, *91*, 1959−1965.
(24) Xia, J.; Masaki, N.; Lira-Cantu, M.; Kim, Y.; Jiang, K.; Yanagida, S. *J. Am. Chem. Soc.* **2008**, *130*, 1258−1263.
(25) Wang, P.; Zakeeruddin, S. M.; Moser, J. E.; Nazeeruddin, M. K.; Sekiguchi, T.; Grätzel, M. *Nat. Mater.* **2003**, *2*, 402−407.